



2

NRL Memorandum Report 6240

**AD-A200 319**

**Investigation of Collisional Effects in the Plasma  
Erosion Opening Switch**

J. M. GROSSMANN, J. M. NERI AND P. F. OTTINGER

*Plasma Technology Division  
Plasma Physics Division*

R. KULSRUD

*JAYCOR  
1608 Spring Hill Rd.  
Vienna, VA 22180-2270*

**DTIC**  
**ELECTE**  
**S** OCT 25 1988 **D**  
**D** C

September 20, 1988

## REPORT DOCUMENTATION PAGE

1a. REPORT SECURITY CLASSIFICATION UNCLASSIFIED		1b. RESTRICTIVE MARKINGS	
2a. SECURITY CLASSIFICATION AUTHORITY		3. DISTRIBUTION / AVAILABILITY OF REPORT Approved for public release; distribution unlimited.	
2b. DECLASSIFICATION / DOWNGRADING SCHEDULE		5. MONITORING ORGANIZATION REPORT NUMBER(S)	
4. PERFORMING ORGANIZATION REPORT NUMBER(S) NRL Memorandum Report 6240		7a. NAME OF MONITORING ORGANIZATION	
6a. NAME OF PERFORMING ORGANIZATION Naval Research Laboratory	6b. OFFICE SYMBOL (If applicable) Code 4770	7b. ADDRESS (City, State, and ZIP Code)	
6c. ADDRESS (City, State, and ZIP Code) Washington, DC 20375-5000		9. PROCUREMENT INSTRUMENT IDENTIFICATION NUMBER	
8a. NAME OF FUNDING / SPONSORING ORGANIZATION DOE	8b. OFFICE SYMBOL (If applicable)	10. SOURCE OF FUNDING NUMBERS	
8c. ADDRESS (City, State, and ZIP Code) Washington, DC 20545		PROGRAM ELEMENT NO.	PROJECT NO.
		TASK DE AI NO 08 79 DP40092	WORK UNIT ACCESSION NO. DN680-382
11. TITLE (Include Security Classification) Investigation of Collisional Effects in the Plasma Erosion Opening Switch			
12. PERSONAL AUTHOR(S) Grossmann, J.M., Kulsrud, * R., Neri, J.M. and Ottinger, P.F.			
13a. TYPE OF REPORT Interim	13b. TIME COVERED FROM TO	14. DATE OF REPORT (Year, Month, Day) 1988 September 20	15. PAGE COUNT 47
16. SUPPLEMENTARY NOTATION *JAYCOR, 1608 Spring Hill Rd., Vienna, VA 22180-2270			
17. COSATI CODES		18. SUBJECT TERMS (Continue on reverse if necessary and identify by block number)	
FIELD	GROUP	SUB-GROUP	
		Opening switches, Plasma erosion opening switches	
		Anomolous transport in plasma	
19. ABSTRACT (Continue on reverse if necessary and identify by block number)			
<p>During the conduction phase of the plasma erosion opening switch (PEOS), current channels in the main body of the plasma have been observed experimentally to be much wider than the collisionless skin depth. In addition, the maximum current carried by the switch before opening (the conduction current) seems to scale roughly linearly with plasma density, <math>n</math>, and switch length, <math>l</math>. Collisionless PIC code simulations of the plasma switch show current conducted in skin-depth like channels, with the conduction current scaling close to <math>l^{2/3}</math> and <math>n^{1/4}</math>. Here the effect of collisions on the behavior of the PEOS is investigated and shown to bring the PIC simulations and experimental results in closer agreement. In the collisional simulations, wider current channels are observed and the conduction current scales linearly with <math>l</math> and as <math>n^{1/2}</math> with density in anode dominated simulations. Linear scaling with length and density in the cathode dominated case can be inferred.</p>			
20. DISTRIBUTION / AVAILABILITY OF ABSTRACT <input checked="" type="checkbox"/> UNCLASSIFIED/UNLIMITED <input type="checkbox"/> SAME AS RPT. <input type="checkbox"/> DTIC USERS		21. ABSTRACT SECURITY CLASSIFICATION UNCLASSIFIED	
22a. NAME OF RESPONSIBLE INDIVIDUAL John M. Grossman		22b. TELEPHONE (Include Area Code) (202) 767-2298	22c. OFFICE SYMBOL Code 4771

## CONTENTS

I.	INTRODUCTION .....	1
II.	DESCRIPTION OF SIMULATIONS .....	7
III.	RESULTS .....	9
	A. Collisionless Simulations .....	9
	B. Collisional Simulations .....	13
	C. Plasma Injection Velocity Effects .....	17
IV.	CONCLUSION .....	20
	REFERENCES .....	22
	DISTRIBUTION LIST .....	35

Accession for	
NTIS - OMA&I	<input checked="" type="checkbox"/>
DTIC TAB	<input type="checkbox"/>
Unannounced	<input type="checkbox"/>
Justification	
By	
Date	
Approved for release	
Dist	Availability Statement
A-1	

# INVESTIGATION OF COLLISIONAL EFFECTS IN THE PLASMA EROSION OPENING SWITCH

## I. Introduction

Inductive storage devices store energy in the form of magnetic fields rather than electric fields and can, in principle, be made considerably smaller and cheaper than their capacitive counterparts. The plasma erosion opening switch (PEOS) is used in inductive storage applications as a means of pulse compression and voltage multiplication<sup>1-10</sup>. The switch consists of a low density plasma ( $n_0 = 10^{12} - 10^{14} \text{ cm}^{-3}$ ) injected with flow velocity,  $V_p$ , between a transparent outer anode of radius  $r_A$ , and a solid inner cathode of radius  $r_K$ . In experiments on the Gamble I and II generators, the ion species is composed mostly of doubly ionized carbon ions,  $C^{++}$ .<sup>11</sup> The switch plasma conducts the generator current for some period of time while the energy of the generator is stored inductively in the vacuum transmission line between the generator and the plasma. The conduction phase ends when the current in the switch reaches a level determined by plasma conditions and the geometry of the switch region.<sup>12</sup> At this predetermined current, the plasma ceases to act as a low impedance short to ground and current is rapidly diverted to the load (opening phase). This opening is accomplished by magnetic insulation of electron flow in a gap formed at the cathode,<sup>13</sup> presumably by erosion.

It has been observed experimentally that during its conduction phase, the PEOS allows magnetic field to penetrate deeply into the main body of the plasma.<sup>13-15</sup> Both the depth of the penetration and the axial width of the current channel

induced in the plasma are many times wider than the collisionless skin depth. In fact, the conduction phase ends and the switch opens only when the magnetic field has penetrated the entire plasma. This phenomenon has provoked a great deal of theoretical interest. The problem is also of interest because of its application to the fusion program and, in particular, to the PBFA II light ion accelerator at Sandia National Laboratory.<sup>8, 16</sup>

Earlier analytic work and simulations of the PEOS using both particle and fluid approaches<sup>17-22</sup> have shown that, in the absence of anomalous collisions, current and magnetic field penetrate the plasma during the conduction phase, but not in the manner expected from experimental observations. Experimental data<sup>13</sup> suggest that: a) current (and magnetic field) penetrates axially in broad channels; b) the penetration of the field at the anode and cathode occurs at almost the same, nearly constant, rate (the current flow is predominantly radial); c) the maximum switch current before opening (the "conduction current") scales almost linearly both with the plasma density,  $n$ , and with the switch length,  $l$ ;<sup>23</sup> and d) switch opening occurs at the cathode. The above scaling agrees with that derived from a model of the switch behavior based on a bipolar emission description of cathode physics which predicts that the conduction current scales linearly both with the plasma flux,  $nV_f$ , and the switch area,  $2\pi r_k l$ .<sup>12</sup>

In several respects, collisionless simulations differ from this experimental picture. First of all, the penetration of the

magnetic field occurs at different rates and via distinct mechanisms near the cathode and the anode. Although separate mechanisms may be responsible for field penetration at the anode and cathode in experiments, penetration has always been observed to occur at nearly the same rate. In collisionless simulations, ions near the cathode are accelerated in the axial direction via  $J \times B$  forces and form a space charge density clump moving through the plasma and toward the load (the "piston" effect).<sup>19</sup> This clump of ions serves to concentrate the electrons emitted from a broad area of the cathode into one narrow (on the order of a few skin depths) current channel. The magnetic field near the cathode penetrates more and more deeply into the plasma as the ion clump is accelerated toward the load.

Near the conducting anode, on the other hand, the current channel migrates toward the load by two mechanisms, depending on proximity to the anode. In the body of the plasma, electrons forming the current channel drift radially by the  $E_z \times B_\theta$  drift and toward the load by the  $E_r \times B_\theta$  drift. Directly at the anode, where the axial electric field vanishes, electrons can no longer drift radially, but must move axially toward the load until their gyro-radii become large enough to allow them to cross to the anode. In this manner, magnetic field near the anode penetrates into the plasma by the axial drift of the electron current channel.<sup>18</sup> When the current channel reaches the load end of the plasma, it disconnects from the plasma and the switch opens. At that point, electrons become magnetically insulated and flow toward the load rather than between the electrodes. In the regimes considered

in this paper, the penetration of the magnetic field is faster at the anode than at the cathode, so the conduction time is determined by the mechanism(s) controlling the anode penetration. Two considerations alter the anode dominated picture: a) in a switch which is longer in axial extent and which conducts for a longer time, it is possible that the  $J \times B$  acceleration of the piston at the cathode could control the opening process, and b) the anode may not be a perfect conductor. In experiments, a wire mesh or a set of widely spaced conducting rods define the anode plane in the PEOS, and the  $E_z$  field does not vanish at all points of the anode plane.

Besides the different penetration rates at the electrodes, other disparities with experimental results also exist. As mentioned above, collisionless simulations (both PIC and fluid) show consistently narrow current channels (~ a few skin depths). Analysis of this phenomenon and discussion of some effects near the cathode which may widen the channels are given in Refs. [19], [20], and [22]. In this paper it will be shown that conduction currents scale roughly like  $l^{2/5}$  and  $n^{1/4}$  in the collisionless PI simulations, rather than scaling linearly as observed experimentally. In addition, the conduction current in collisionless simulations will be seen to be insensitive to plasma flux. Since these simulation results compare poorly with experiment, it is concluded that the conduction physics in the collisionless simulations is different from the one operating in experiment.

It has long been speculated that an anomalous collision mechanism exists in the plasma and is responsible for the broad current channel observed in experiments.<sup>12,13,24,25</sup> Beside the usual instabilities, such as the Buneman, ion-acoustic, etc., which may be active in the switch, another electrostatic instability has been recently identified with many germane properties.<sup>26</sup> This mode has a linear growth time ( $\tau_s \sim 7/\omega_{p1}$ ) of about 2-3 ns for typical experimental parameters; its effective collision frequency is large ( $\nu_s \leq 0.4\omega_{p0}$ ) because it is weakly saturated and grows to large amplitudes; finally, the mode propagates at the ion acoustic speed so that it can achieve this large amplitude without convecting out of the plasma during the time of interest. Simulations are currently being conducted to investigate this instability further, especially its non-linear behavior and dependence on plasma parameters. To include this instability self-consistently into the current class of two (spatial) dimensional particle codes is impossible because the unstable wave requires a component in the third dimension. Even with a three dimensional code, a completely self-consistent treatment of the problem may be difficult and expensive. The dimensions associated with experimental geometries is large compared with the cell sizes needed to resolve the cathode emission process and the wavelength of the unstable modes. A large number of macro-particles per cell are also necessary to resolve the Maxwellian distribution and provide enough electrons resonant with the unstable wave. For these reasons, an ad hoc method will be used here to include the effect of the instability in the PIC

simulations of the PEOS problem. The use of a particle code in the  $r - \theta$  plane to examine the instability in a small volume will be the subject of a future paper.

In the present treatment, a time varying region is chosen where the instability is assumed to be active and then a collision frequency,  $\nu_c$ , is selected. The collision term is incorporated in the electron equations of motion so that electrons are subjected to a damping force  $-\nu_c m \gamma V$ , where  $\gamma$  is the relativistic factor. The collision frequency is chosen to be within the range of values predicted by the instability analysis, but its exact value and its region of influence are not chosen self-consistently or with reference to turn-on conditions, turn-off, saturation, etc. The underlying motive is to discover what effect such an instability would have on the behavior of the PEOS. Thus the purpose of this paper is not to prove that such an instability exists or to study the exact details of its effect, but to show that its presence could alter the behavior of the simulated switches so that they operate more like those observed experimentally.

The effects of anomalous resistivity have been investigated previously in particle and fluid simulations of the PEOS.<sup>22, 25, 27-29</sup> Although not treating the instability described above, the usual streaming, ion acoustic, and lower hybrid instabilities have been modeled in detail by including the appropriate transport coefficients.<sup>28, 29</sup> Compared to collisionless results, these simulations have shown improved

agreement with experiment concerning channel widths and penetration velocity. In this paper, a more general study of anomalous collision effects is made, with the focus on scaling of PEOS operation with length, density, and plasma injection velocity for a fixed collision rate. Scaling studies are also performed for collisionless simulations and compared with the collisional results.

## II. Description of Simulations

The work presented in this paper treats the conduction of current through a low density ( $n_0 \sim 0.25-4 \times 10^{12} \text{ cm}^{-3}$ ) plasma injected between two coaxial conducting cylinders as shown in Fig. 1. The plasma is injected through the anode toward the cathode with flow velocity,  $V_p$ , and is assumed to be azimuthally symmetric. The coaxial electrodes and the switch plasma form part of a circuit with the generator at the left and a load in parallel with the switch at the right. In the present simulations where the focus is on the conduction phase of the switch, the load is chosen to be a short circuit. The regions on both sides of the plasma between the plasma and the axial boundaries are in vacuum. An electromagnetic pulse is driven into the system from the left and induces current in the plasma. Current rises to about 120 kA in 5 ns. The time scale of 5 ns is chosen to reduce the computation time. To partially compensate for this artificially small time scale, the ion species is chosen to be hydrogen,  $H^+$ , rather than carbon,  $C^{++}$ .

Space charge limited electron emission is allowed on the conducting surfaces and particles that encounter the surfaces are absorbed. The 2-1/2D electromagnetic particle-in-cell code "MASK"<sup>30</sup> is used to treat the switch plasma, the boundary emission of electrons into the plasma, and the initial flow of plasma into the simulation region. The problem is done in r-z geometry and azimuthal symmetry is imposed. Three separate issues are addressed here. These are conduction current scaling with length, density, and plasma flow velocity.

Scaling simulations are run with and without anomalous collisions. Anomalous collisions are introduced in regions of the plasma in which the magnetic field is above a certain threshold ( 10% of the maximum B field at any given time) by turning on the collisional term  $-v_e m_e \gamma V$  in the particle equations of motion. The magnetic field is used as a turn on condition because its presence signals that current is being driven through the plasma which, in turn, can drive the instability. As mentioned earlier, the motivation here is to determine whether collisional simulations of the switch more closely resemble experimentally observed scalings.

Although the length, density, and plasma flow velocity are varied in the simulations discussed herein, the same driving current waveform (rising linearly to about 120 kA in 5 ns), the same radial dimensions ( $r_k = 2.5$  cm,  $r_A = 5$  cm), and the same collision frequency (in the collisional runs),  $\nu_e = 1.0 \times 10^{10}$  s<sup>-1</sup>,

are used in all cases. There was no attempt to scale  $v_e$  with density, magnetic field, or other parameter as dictated by any given instability. However, for reference purposes, note that the ratio  $v_e/\omega_p$  varies from 0.09 for  $n_0 = 4 \times 10^{12} \text{ cm}^{-3}$  to 0.35 for  $n_0 = 2.5 \times 10^{11} \text{ cm}^{-3}$ .

### III. Results

This section begins with an examination of length and density scaling for the series of simulations described in Table I. The discussion is broken into two sections, one devoted to collisionless, the other to collisional results. These two sections are followed by a third concerning the effects of varying the injection velocity.

#### A. Collisionless Simulations

In Fig. 2, the motion of the current front,  $D(t)$ , is plotted as a function of time for the case where  $n = 10^{12} \text{ cm}^{-3}$ ,  $l = 10 \text{ cm}$  and  $V_e = 1.8 \times 10^8 \text{ cm/s}$ . The position of the current front near the anode ( $r = 4.5 \text{ cm}$ ) and near the cathode ( $r = 3.0 \text{ cm}$ ) are plotted separately. The current front position is defined to be the axial position where  $B_\theta$  begins to rise from zero. A least squares power curve fit is used on the data points. The current penetration distance during the first 0.4 ns is not represented accurately in these curves because the initial penetration,  $\delta$ ,

occurs rapidly over the distance of a few skin depths,  $\delta = 2.4$  cm.

The anode and cathode curve fits,  $D_A(t)$  and  $D_K(t)$ , are tabulated in Table I, case (a). The anode front scales as  $t^{2.8}$ , while the cathode front as  $t^{2.5}$ . Since the current rises linearly in time, and the switch opens in this simulation when the anode front reaches the load end of the plasma ( $D_A(t) = 1$ ), it is inferred that the conduction current scales with length roughly as  $l^{1/2.8}$ . Similar scaling can be done for all the other collisionless runs shown in Table I (cases (b) - (e)). Taking a rough average of all the exponents of time in the function  $D_A(t)$ , the conduction current scales roughly as  $l^{2/5}$  with length in the collisionless case.

In Fig. 3, the current front position is shown for the case of a higher density plasma,  $n = 4 \times 10^{12} \text{ cm}^{-3}$ ,  $l = 10 \text{ cm}$ , and  $V_f = 1.8 \times 10^8 \text{ cm/s}$ . The initial penetration is reduced to  $\delta = 1.1 \text{ cm}$ , and the anode penetration curve scales as  $t^{2.3}$  with time, as seen in Table I, case (b). The functional dependence of the cathode end of the current channel on time varies strongly as the density changes from  $10^{12} \text{ cm}^{-3}$  to  $4 \times 10^{12} \text{ cm}^{-3}$ . As shown in Table I,  $D_K(t) \sim 0.5t^{2.5}$  for  $n_0 = 10^{12} \text{ cm}^{-3}$ , while  $D_K(t) \sim 0.25t^{1.4}$  for  $n_0 = 4 \times 10^{12} \text{ cm}^{-3}$ . Cathode penetration for the  $n_0 = 4 \times 10^{12} \text{ cm}^{-3}$  case follows the axial penetration of a leaky piston accelerated by  $J \times B$  forces through the plasma.<sup>19</sup> However, at  $n_0 = 10^{12} \text{ cm}^{-3}$ , the current front position and piston do not track because a small amount of current is able to penetrate 4-5 cm

ahead (toward the load) of the piston. The amount of current more than 1 cm in front of the piston is less than 30% of the total carried by the switch, and the amount of current more than 2 cm in front is less than 15% of the total. So the piston still defines the most active region of electron emission. The piston in the  $n_0 = 10^{12} \text{ cm}^{-3}$  run depends on time roughly as the function  $0.4t^{1.4}$ .

Several other regimes of density and length have been examined and results are shown in Table I, together with estimates of the scaling of conduction current with density. All cases in Table I have  $V_p = 1.8 \times 10^8 \text{ cm/s}$ . Comparing the two  $l = 5 \text{ cm}$  cases ((d) and (e)), at  $n_0 = 10^{12} \text{ cm}^{-3}$  and  $4 \times 10^{12} \text{ cm}^{-3}$ , we find from the actual time when opening begins,  $\tau_0$ , that the conduction current scales as  $n^{1/4}$ . The density scaling is obtained by assuming that  $I_0 \sim \tau_0 \sim n^\alpha$  for a linearly rising current drive. When a correction is made for the different initial penetration depths (2.4 cm and 1.1 cm, respectively), the conduction time scales more like  $n^{1/7}$ . The corrected scaling is obtained by assuming the same initial penetration depth (2.4 cm for (a), (b) and (c), 2.5 cm for (d) and (e)) applies to the cases to be compared. A new estimated opening time is found by solving  $D_\lambda(\tau) = 1$  for  $\tau_0$  (with the modified  $\delta$ ), and then used to scale. This scaling more accurately reflects the actual penetration velocity through the plasma after the initial current penetration has occurred. Corrected scalings for  $l = 10 \text{ cm}$  comparing  $n_0 = 10^{12}$ ,  $4 \times 10^{12}$ , and  $2.5 \times 10^{11} \text{ cm}^{-3}$  show scaling as  $n^{1/4}$ .

The conclusions reached above for length and density scaling pertain to collisionless switch simulations for which anode current penetration dominates cathode penetration. Collisionless simulations of the switch using the implicit code "ANTHEM" in the parameter regimes of Gambles I and II ( $\tau \approx 50$  ns,  $C^{++}$  plasma) with a conducting anode also show opening dominated by anode penetration,<sup>29</sup> so the conclusions obtained here for a  $\tau = 3-5$  ns,  $H^+$  plasma should apply to the Gamble regimes. For a longer conduction time switch (i.e.,  $\tau_0 > 100$  ns with a  $C^{++}$  carbon plasma),  $J \times B$  acceleration of the ion piston could dominate the opening process in a collisionless simulation of the switch and stronger scaling with density and length would be seen. The same remark applies to the case when the anode is not a perfect conductor. If cathode penetration ( $D_K(t)$ ) determined the opening time in these simulations, one would find nearly linear corrected scaling with density when comparing  $n_0 = 10^{12}$   $cm^{-3}$  and  $n_0 = 4 \times 10^{12}$   $cm^{-3}$  (with  $\delta = 2.4$  cm,  $l = 10$  cm). However, when comparing  $n_0 = 2.5 \times 10^{11}$   $cm^{-3}$  and  $n_0 = 10^{12}$   $cm^{-3}$ , the scaling becomes  $n^{0.4}$ . This change in the scaling may be the result of the effect described earlier, namely that the cathode current front tracks the piston at high densities but can move slightly ahead of the piston at low densities. Conduction current scaling with length can also be inferred from the indices of time in the functions  $D_K(t)$ . Again the scaling for the  $l = 10$  cm runs seems to be a function of the density regime. At densities of  $10^{12}$   $cm^{-3}$  or lower, the conduction current would scale roughly as  $l^{1/2.3}$ , while at  $n_0 = 4 \times 10^{12}$   $cm^{-3}$  it scales as  $l^{1/1.4}$ .

Summarizing the collisionless results, it is concluded that conduction current scales roughly as  $l^{2/5}$  with length and as  $n^{1/4}$  with density in this anode dominated regime. Stronger scalings are found from the cathode penetration distances. However, the scaling is dependent on the density regime. At the cathode, current penetrates primarily by the axial  $J \times B$  acceleration of a leaky ion piston, while at the anode axial  $E \times B$  drift of electrons moves the front toward the load. The current channels observed in collisionless runs are usually about 1 cm wide for  $n_0 = 4 \times 10^{12} \text{ cm}^{-3}$ , 1.5-2.5 cm wide for  $n_0 = 10^{12} \text{ cm}^{-3}$ , and 3-4.5 cm for  $n_0 = 2.5 \times 10^{11} \text{ cm}^{-3}$ . These widths are about 3-4 skin depths at the various densities.

The anode penetration distances presented here depend on time to some power greater than two, while similar distances presented in Ref. [19] depend logarithmically. This apparent discrepancy is a result of the radial location of the measurement. In the present paper, the axial penetration distance is measured at  $r = 4.5 \text{ cm}$ . In the previous work it was taken at  $r = 5.0 \text{ cm}$  where the axial  $E \times B$  drift dominates because  $E_z$  and the radial  $E \times B$  drift vanish at the conducting anode. These differences again give an indication of how important the anode boundary conditions are.

#### B. Collisional Simulations

Current penetration distances from three collisional

simulations are shown in Fig. 4. The parameters used are outlined in Table I, cases (f)-(h). Only the first 3.2 ns of the  $n_0 = 4 \times 10^{12} \text{ cm}^{-3}$  run are shown. In the lower density regimes, the anode and cathode currents migrate through the plasma at approximately the same rate, so only one curve is drawn. At higher densities ( $> 2 \times 10^{12} \text{ cm}^{-3}$ ), the penetration rates are different. This occurs because the collisional frequency  $\nu_a = 10^{10} \text{ s}^{-1}$  used in the higher density cases is not sufficient to prevent the JxB piston effect described in the introduction. When a higher collision frequency,  $\nu_a = 2 \times 10^{10} \text{ s}^{-1}$ , is used in the  $n_0 = 4 \times 10^{12} \text{ cm}^{-3}$  case, anode penetration remains almost the same as for  $\nu_a = 10^{10} \text{ s}^{-1}$ , but cathode penetration proceeds at a faster pace. At  $t = 3.2 \text{ ns}$  with  $\nu_a = 2 \times 10^{10} \text{ s}^{-1}$ , the cathode current channel is 0.8 cm behind the anode current channel, while with  $\nu_a = 10^{10} \text{ s}^{-1}$ , the channels are separated axially by 1.3 cm. That collisions have a more substantial effect at the cathode than at the anode is consistent with earlier conjecture that anomalous collisions at the cathode alone may be sufficient to cause broad channels and a deeply penetrating magnetic field.<sup>22,25</sup>

The first observation from Fig. 4 is that the penetration is linear in time rather than a power of time. The conduction current therefore scales linearly with switch length. Figure 4 also shows that the rate of penetration is more strongly dependent on the density than in the collisionless simulations. As detailed in Table I, the slope of the anode curve is 2.9 cm/ns at  $n_0 = 10^{12} \text{ cm}^{-3}$ , while it is 1.34 cm/ns at  $n_0 = 4 \times 10^{12} \text{ cm}^{-3}$

and 2.2 cm/ns at  $n_0 = 2 \times 10^{12} \text{ cm}^{-3}$ . At the lower density,  $n_0 = 2.5 \times 10^{11} \text{ cm}^{-3}$ , the slope is 4.9 cm/ns. The scalings for these cases show that the conduction time scales roughly as  $n^{1/2}$  in the anode dominated case.

If the conduction process were cathode dominated (because the anode is not a perfect conductor, for example), then even stronger scalings would apply. According to the  $D_k(t)$  curves in the collisional case, conduction current scaling is linear in both density and length. In contrast to the collisionless case, these scalings are independent of density regime. The mechanism behind cathode penetration in the collisional simulations is no longer axial  $J \times B$  acceleration as in the collisionless cases. The scaling of cathode penetration with density and length suggests that the mechanism is related to bipolar space charge limited emission as described in.<sup>12</sup>

An additional important observation concerning the collisional results is that, as found in previous work, the current channels are wider than in the collisionless regime. It is found that for a 10 cm plasma, channel widths of 7-9 cm are typical. The current is spread fairly uniformly early in a simulation, but becomes somewhat more concentrated near the generator side of the plasma late in time after plasma density accumulates in a weak ion piston which forms near the cathode. In Figs. 5 - 7, a comparison is made between collisionless and collisional results. The figures are taken from cases (a) and (f) of Table I. The axial length of the region shown is 12.8 cm.

and its radial height is 2.5 cm. Dashed vertical lines in the simulation region define the boundary of the original plasma fill. Figure 5 shows magnetic field contours at  $t = 2.4$  ns for the collisionless and the collisional case. The contour levels are the same in both plots and vary from  $-4.5$  kG (level 1) to  $-55.56$  G (level 9) with an increment of  $0.55$  kG per level. The figure shows that the magnetic field is spread uniformly over a width of about  $7.6$  cm in the collisional simulations, with a slight concentration of current near the generator side of the plasma. In the collisionless simulations, current is carried diagonally between the electrodes in a channel of width  $\sim 2$  cm.

In Figs. 6 and 7, electron and ion particle plots compare results from the collisionless and collisional simulations at  $t = 2.4$  ns. As reported in earlier work,<sup>19</sup> in the collisionless case electrons  $E \times B$  drift diagonally between the electrodes, with the electric field in the drift channel produced largely by net positive space charge to the left of the diagonal electron current channel. Ion charge accumulates near the cathode in a diagonal piston which  $J \times B$  accelerates axially toward the load.

In contrast, the electron flow in the collisional case (see Figs. 5 (b) and 6(b)), is predominantly radial and spread throughout the plasma. Certain effects from the collisionless regime are also manifest. For example, diagonal flow is established at the generator edge of the plasma, but some electrons spiral in an  $E \times B$  drift which does not allow them to cross to the anode. That no current crosses to the anode at the generator side of the plasma can be seen by studying Figs. 5(b) and 6(b). As in the collisionless regime, the electric field

responsible for the ExB drift is produced by space charge separation. Also, a piston forms in the ions even in the collisional case, although generally it is smaller and takes a few nanoseconds longer to appear.

### C. Plasma Injection Velocity Effects

An examination has been made of the sensitivity of the current penetration velocity on the plasma injection velocity,  $V_p$ . Although no direct experimental evidence exists for this scaling, the NRL theory<sup>1,2</sup> of current penetration velocity scaling with  $V_p$  suggests that it should be linear, with a correction factor depending on the ratio of the cathode gap potential,  $e\phi$ , to the ion injection energy  $M_i V_p^2/2$ .<sup>20</sup> The space charge limited current density is given by,

$$j_{scl} = \alpha j_{bp} \quad (1)$$

$$\text{where } \alpha = \frac{\sqrt{1+F} - 1}{\sqrt{F}} \quad (2)$$

$$\text{and } F = \frac{2Ze\phi}{M_i V_p^2} \quad (3)$$

Here  $Z$  is the ion charge state and  $M_i$  the ion mass. In Eq.(1),  $j_{bp}$  is the usual bipolar current density relating the electron current density to the smaller ion current density,  $n_i ZeV_p$ , so that,

$$j_{bp} = \sqrt{\frac{M_i}{Zm_e}} n_i Z e V_F \quad (4)$$

Note that the correction factor,  $\alpha$ , results from injecting ions into the accelerating gap with non-zero energy. From Eqs. (1)-(4), a  $10^{12} \text{ cm}^{-3}$ ,  $\text{H}^+$  plasma of length  $l = 5 \text{ cm}$ , injected at  $V_F = 1.8 \times 10^8 \text{ cm/s}$  into the system depicted in Fig. 1 is expected to conduct approximately  $I_0 = 65 \text{ kA}$  before opening (assuming that  $n_i = 10^{12} \text{ cm}^{-3}$  at the cathode and that the gap potential  $\phi = 10^5 \text{ V}$ , as is typical in the simulations). In the collisionless and collisional simulations, however,  $I_0 = 37 \text{ kA}$ , suggesting that other factors also affect the conduction current  $I_0$ . Scaling with  $V_F$  can still be tested by assuming that  $I_0 = 37 \text{ kA}$  is the space charge limited current for  $V_{F0} = 1.8 \times 10^8 \text{ cm/s}$  and then injecting  $V_F = 4V_{F0}$  and  $V_F = V_{F0}/4$  to see if  $I_0$  increases or decreases incrementally as expected from Eqs. (1)-(4). The results are shown in Table II. From left to right in the table are the collision frequency, injection velocity, cathode gap potential, the factor  $\alpha$  from Eq. (2), and the predicted conduction current,  $I_s^P$ . The current  $I_s^P$  is found by using Eqs. (1)-(4) and then adding the ion current at the cathode in order to obtain the full conduction current,  $I_s^P = I_0 + I_1$ . Because  $r_K = r_A/2$  and because the initial plasma density is uniform in  $r$ , the cathode ion current is one half the ion current injected at the anode,  $I_F$ , shown in the next column in Table II. A comparison of  $I_s^P$  to the actual conduction current,  $I_0$ , in the right-most column shows poor correspondence in both the

collisional and collisionless regimes. Little change is observed in  $I_0$  as  $V_p$  is varied in the collisionless regime. Collisional results do show sensitivity to  $V_p$ , but the scaling is weaker than expected from Eqs. (1)-(4).

In the collisional runs, a curious correspondence exists between the additional conduction current carried by the simulated PEOS and the additional ion current,  $I_p$ , injected at the anode into the system. Of course, both electrons and ions are injected at the anode with the same injection velocity, but many electrons begin to ExB drift axially so that a radial ion current  $I_p = 2\pi r_A n_i Z e V_p$  becomes available near the anode. A simulation of a stationary plasma ( $V_p = 0$ ) shows that it carries conduction current  $I_s = 33$  kA. Using this as a base current, the conduction current due to the additional ion current,  $I_p$ , becomes  $I_1^P$ , shown in the next to last column ( $I_1^P = I_s + I_p$ ). In the collisional regime,  $I_1^P$  predicts the conduction current fairly well for all injection velocities except the  $1.44 \times 10^9$  cm/s case. It is possible that the (initially comoving) electron current is not deflected axially as effectively at these high velocities.

The conclusions reached above apply to the case simulated above where the anode is a perfect conductor. If the anode allowed an axial electric field, electrons could drift radially near the anode and different scaling with  $V_p$  may be seen.

#### IV. Conclusion

An attempt has been made in this paper to reconcile experimental observations and numerical results regarding the conduction phase of the PEOS. Experimentally it is found that current and field penetrate axially into the plasma in wide channels.<sup>13-15</sup> More recently, the conduction current has been observed to scale roughly linearly with plasma length and density.<sup>23</sup> An analytic model of the switch predicts that the conduction current should scale linearly with density, length, and injection velocity.<sup>12</sup> In contrast to these expectations, collisionless simulations of the PEOS in the anode dominated case show narrow channels,  $n^{1/4}$  dependence on density, almost no sensitivity to injection velocity, and  $l^{2/5}$  scaling of the conduction current with length. From an examination of the cathode penetration curves in the collisionless simulations, conduction current scalings with length and density depend on the density regime in question. Generally, the scalings are stronger at the cathode than the anode, but still sublinear. The current penetrates at the cathode by convective  $J \times B$  acceleration of a piston toward the load, although at low densities a small amount of current is able to penetrate ahead of the piston.

When an ad hoc collisional model is introduced in the simulations, agreement with experiment improves. In these anode dominated simulations, conduction current scales linearly with length, as  $n^{1/2}$  with density, and much wider current channels are produced. Although some sensitivity to injection velocity is

seen, the dependence is much weaker than predicted from a space charge limited model of the conduction phase. Even better agreement with experiment is obtained from the cathode penetration curves in the collisional simulations. It can be inferred that if the conduction phase of the switch were cathode dominated, then the conduction current would scale linearly with both length and density. Unlike the collisionless results, these scalings are independent of the density regime being considered. The cathode penetration mechanism in the collisional case is no longer axial  $J \times B$  acceleration, and seems consistent with the NRL model.<sup>1,2</sup>

Future work in this area should confirm the cathode dominated scalings using non-conducting anode boundary conditions. More work is also needed to examine the effects of improved modeling of instabilities, and to understand the weak conduction current scaling with injection velocity.

## References

<sup>1</sup>C.W. Mendel, Jr. and S.A. Goldstein, J. Appl. Phys., 48, 1004 (1977).

<sup>2</sup>R. Stringfield, R. Schneider, R.D. Genuario, I. Roth, K. Childers, C. Stallings, and D. Dakin, J. Appl. Phys., 52, 1278 (1981).

<sup>3</sup>R.A. Meger, R.J. Commisso, G. Cooperstein, and Shyke A. Goldstein, Appl. Phys. Lett., 42, 943 (1983).

<sup>4</sup>S. Miyamoto, N. Yugami, H. Fujita, T. Ozaki, K. Imasaki, S. Nakai, and C. Yamanaka, Jpn. J. Appl. Phys., 25, L108 (1986).

<sup>5</sup>B.V. Weber, R.J. Commisso, G. Cooperstein, J.M. Grossmann, D.D. Hinshelwood, D. Mosher, J.M. Neri, P.F. Ottinger, S.J. Stephanakis, IEEE Trans. Plasma Sci., 15, 635 (1987).

<sup>6</sup>S.P. Bugaev, B.M. Kival'chuk, and G.A. Mesyats, Proc. Sixth Int. Conf. on High-Power Particle Beams (Kobe, Japan), 878 (1986).

<sup>7</sup>J.M. Neri, J.R. Boller, P.F. Ottinger, B.V. Weber, and F.C. Young, Appl. Phys. Lett., 50, 1331 (1987).

<sup>8</sup>R.W. Stinnett, D.H. McDaniel, G.E. Rochau, W.B. Moore, E.W. Gray, T.J. Renk, H.N. Woodall, T.W. Hussey, S.S. Payne, R.J. Commisso, J.M. Grossmann, D.D. Hinshelwood, R.A. Meger, J.M. Neri, W.F. Oliphant, P.F. Ottinger, and B.V. Weber, IEEE Trans. Plasma Sci., 15, 557 (1987).

<sup>9</sup>H. Bluhm, K. Boehnel, P.Hoppe, H.U. Karow, and D. Rusch, IEEE Trans. Plasma Sci., 15, 654 (1987).

<sup>10</sup>C. Bruno, J. Delvaux, A. Nicolas, and M. Roche, IEEE Trans. Plasma Sci., 15, 686 (1987).

<sup>11</sup>R.J. Commisso, D.D. Hinshelwood, J.M. Neri, W.F. Oliphant, and B.V. Weber, NRL Memorandum Report 6057, (1987).

<sup>12</sup>P.F. Ottinger, S.A. Goldstein, and R.A. Meger, J. Appl. Phys., 56, 774 (1984).

<sup>13</sup>B.V. Weber, R.J. Commisso, R.A. Meger, J.M. Neri, W.F. Oliphant, and P.F. Ottinger, Appl. Phys. Lett., 45, 1043 (1984).

<sup>14</sup>D.D. Hinshelwood, J.R. Boller, R.J. Commisso, G. Cooperstein, R.A. Meger, J.M. Neri, P.F. Ottinger, and B.V. Weber, Appl. Phys. Lett., 49, 1635 (1986).

<sup>15</sup>D.D. Hinshelwood, J.R. Boller, R.J. Commisso, G. Cooperstein, R.A. Meger, J.M. Neri, P.F. Ottinger, and B.V. Weber, IEEE Trans. Plasma Sci., 15, 564 (1987).

<sup>16</sup>J.P. VanDevender and D.L. Cook, *Science*, 232, 831 (1986).

<sup>17</sup>E.M. Waisman, P.G. Steen, D.E. Parks, and A. Wilson, *Appl. Phys. Lett.*, 46, 1045 (1985).

<sup>18</sup>J.M. Grossmann, J.M. Neri, P.F. Ottinger, and A.T. Drobot, *Bull. Am. Phys. Soc.*, 29, 1207 (1984); J.M. Grossmann, P.F. Ottinger, J.M. Neri, D. Mosher, and A.T. Drobot, *Bull. Am. Phys. Soc.*, 30, 1448 (1985).

<sup>19</sup>J.M. Grossmann, P.F. Ottinger, J.M. Neri, and A.T. Drobot, *Phys. Fluids*, 29, 2724 (1986).

<sup>20</sup>D. Mosher, J.M. Grossmann and P.F. Ottinger, *IEEE. Trans. Plasma Sci.*, 15, 695 (1987).

<sup>21</sup>R.J. Mason, J.M. Wallace, and K. Lee, *Proc. of the 6th Int. Conf. on High Power Particle Beams*, (Kobe, Japan), 295 (1986).

<sup>22</sup>J.M. Grossmann, D. Mosher, and P.F. Ottinger, *IEEE Trans. Plasma Sci.*, 15, 704 (1987).

<sup>23</sup>B.V. Weber, R.J. Comisso, P.J. Goodrich, D.D. Hinshelwood, W.F. Oliphant, and P.F. Ottinger, *Bull. Am. Phys. Soc.*, 32, 1878 (1987).

<sup>24</sup>P.F. Ottinger, R.M. Kulsrud, J.M. Grossmann, R.J. Commisso, D.G. Colombant, D.D. Hinshelwood, D. Mosher, J.M. Neri, and B.V. Weber, Bull. Am. Phys. Soc., 31, 1443 (1986).

<sup>25</sup>J.M. Grossmann, P.F. Ottinger, D. Mosher, D.G. Colombant, J.M. Neri, B.W. Weber, D.D. Hinshelwood, and R.J. Commisso, Bull. Am. Phys. Soc., 31, 1444 (1986).

<sup>26</sup>R. Kulsrud, P.F. Ottinger, and J.M. Grossmann, Bull. Am. Phys. Soc., 32, 1878 (1987); also to be published in Phys. Fluids.

<sup>27</sup>D. Colombant, J.M. Grossmann, and P.F. Ottinger, Bull. Am. Phys. Soc., 30, 1447 (1985).

<sup>28</sup>S.S. Payne, T.W. Hussey, R.W. Stinnett, and N.F. Roderick, IEEE Trans. Plasma Sci., 15, 725 (1987).

<sup>29</sup>R.J. Mason, J.M. Wallace, J.M. Grossmann, and P.F. Ottinger, IEEE Trans. Plasma Sci., 15, 715 (1987).

<sup>30</sup>A.T. Drobot, Bull. Am. Phys. Soc., 29, 1379 (1984).

Table I. Anode ( $D_A$ ) and cathode ( $D_K$ ) penetration distances and conduction times ( $\tau_0$ ) for various collisionless and collisional runs.

run	$\nu \times 10^{10}$ ( $s^{-1}$ )	$n \times 10^{12}$ ( $cm^{-3}$ )	$l$ (cm)	$D_A(t)$ (cm)	$D_K(t)$ (cm)	$\tau_0$ (ns)
a	0	1.0	10	$2.4 + 0.66t^{2.3}$	$2.4 + 0.47t^{2.5}$	2.4
b	0	4.0	10	$1.1 + 0.34t^{2.3}$	$1.1 + 0.26t^{1.4}$	4.0
c	0	0.25	10	$4.4 + 2.4t^{2.2}$	$4.4 + 2.2t^{2.2}$	1.45
d	0	1.0	5	$2.5 + 0.64t^{2.4}$	$2.5 + 0.56t^2$	1.8
e	0	4.0	5	$1.2 + 0.31t^{2.7}$	$1.2 + 0.21t^{1.8}$	2.6
f	1	1.0	10	$1.3 + 2.9t$	$1.3 + 2.9t$	3.0
g	1	4.0	10	$0.7 + 1.34t$	$1.3 + 0.74t$	6.9
h	i	0.25	10	$3.3 + 4.9t$	$3.3 + 4.9t$	1.4
i	1	2.0	10	$1.1 + 2.2t$	$1.37 + 1.5t$	3.8

Table II. Conduction currents ( $I_o$ ) at different injection velocities ( $V_F$ ) for various collisionless and collisional runs.

run	$\nu \times 10^{10}$ ( $s^{-1}$ )	$V_F \times 10^8$ (cm/s)	$\Phi$ (kV)	$\alpha$	$I_S^P$ (kA)	$I_F$ (kA)	$I_i^P$ (kA)	$I_o$ (kA)
a	0	1.8	85	0.65	-	4.5	-	37.5
b	0	7.2	89	0.27	64.5	18.1	51.1	39.0
c	1.0	1.8	100	0.67	-	4.5	37.5	37.5
d	1.0	7.2	100	0.28	66.7	18.1	51.1	50
e	1.0	0.45	77	0.89	12.5	1.13	34.1	34.0
f	1.0	14.4	100	0.15	76.2	36.2	69.2	56.3

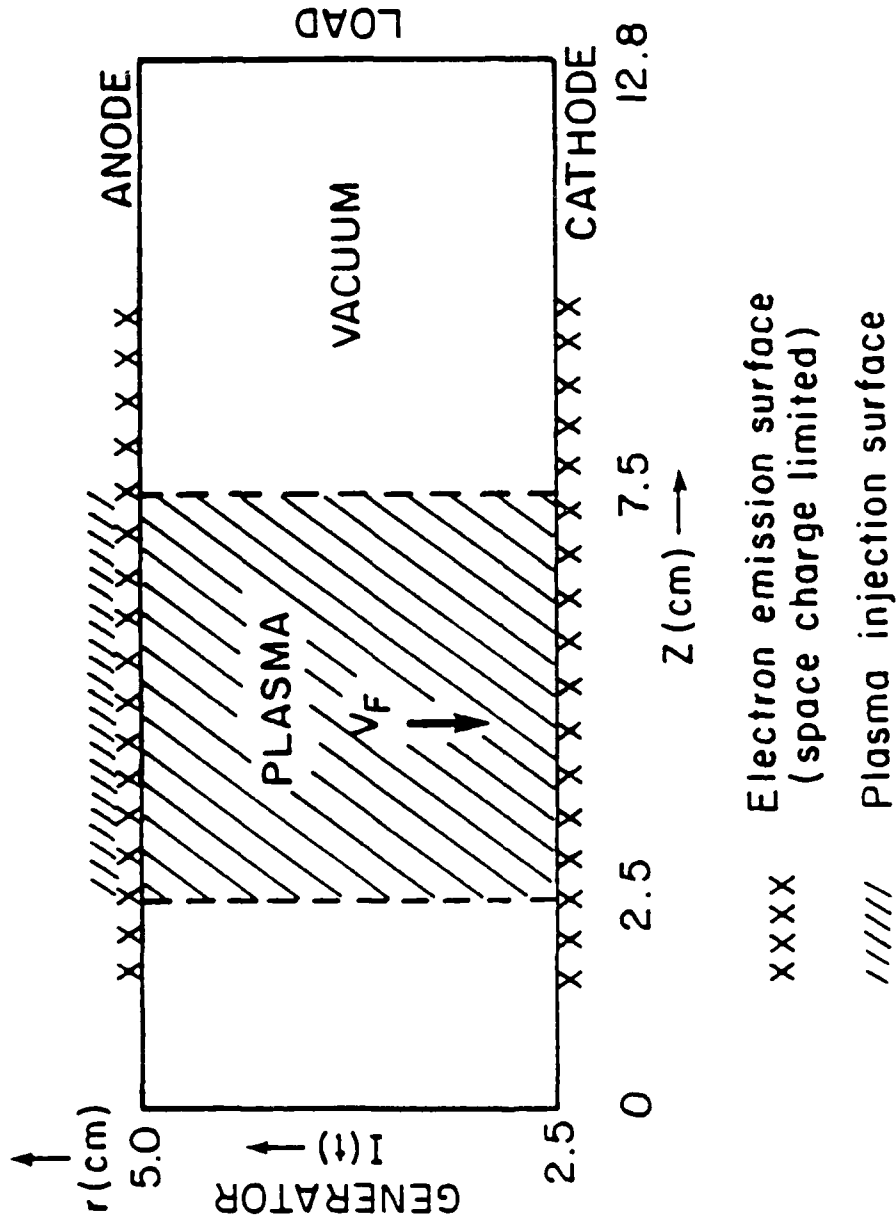


Fig. 1. Simulation region showing components of typical PEOS system. A short circuit load is used in these simulations.

# MOTION OF CURRENT FRONT

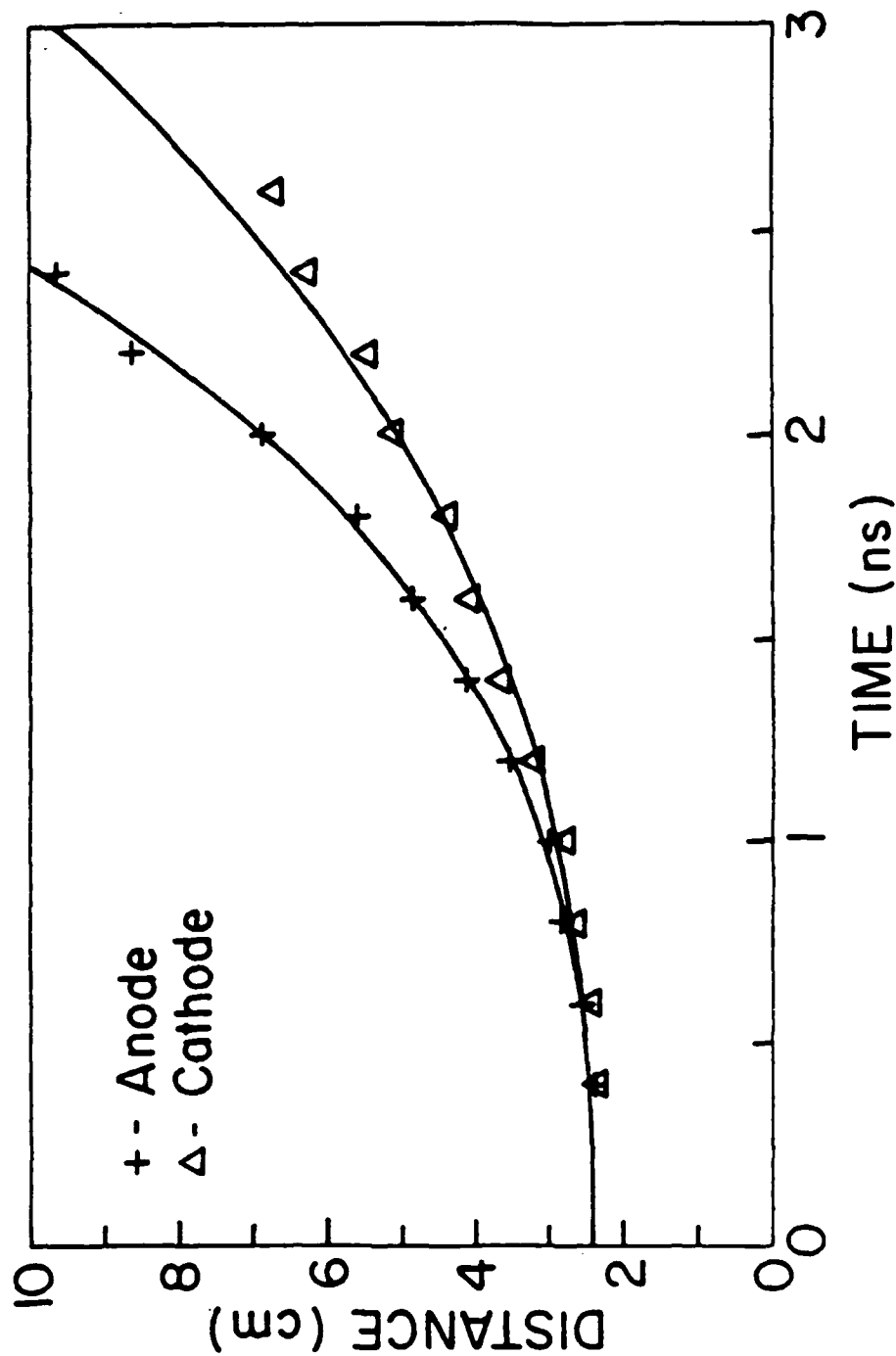


Fig. 2. Anode and cathode penetration as a function of time for run (a) of Table I. The solid lines are least square power curve  $(a + bt^\alpha)$  fits of the simulation data.

# MOTION OF CURRENT FRONT

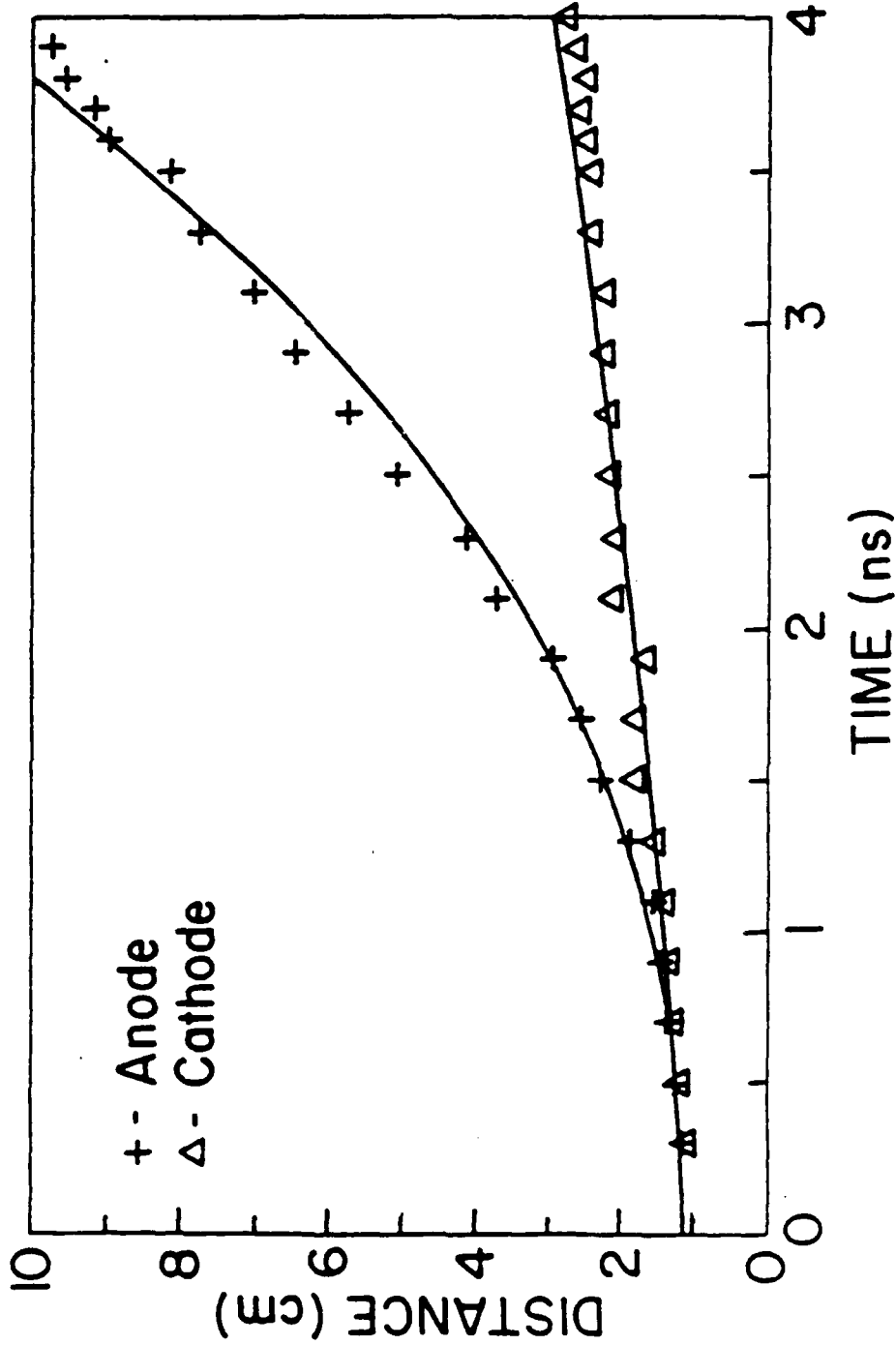


Fig. 3. Anode and cathode penetration as a function of time for run (b) of Table I. Solid lines are least square fits of simulation data.

# MOTION OF CURRENT FRONT

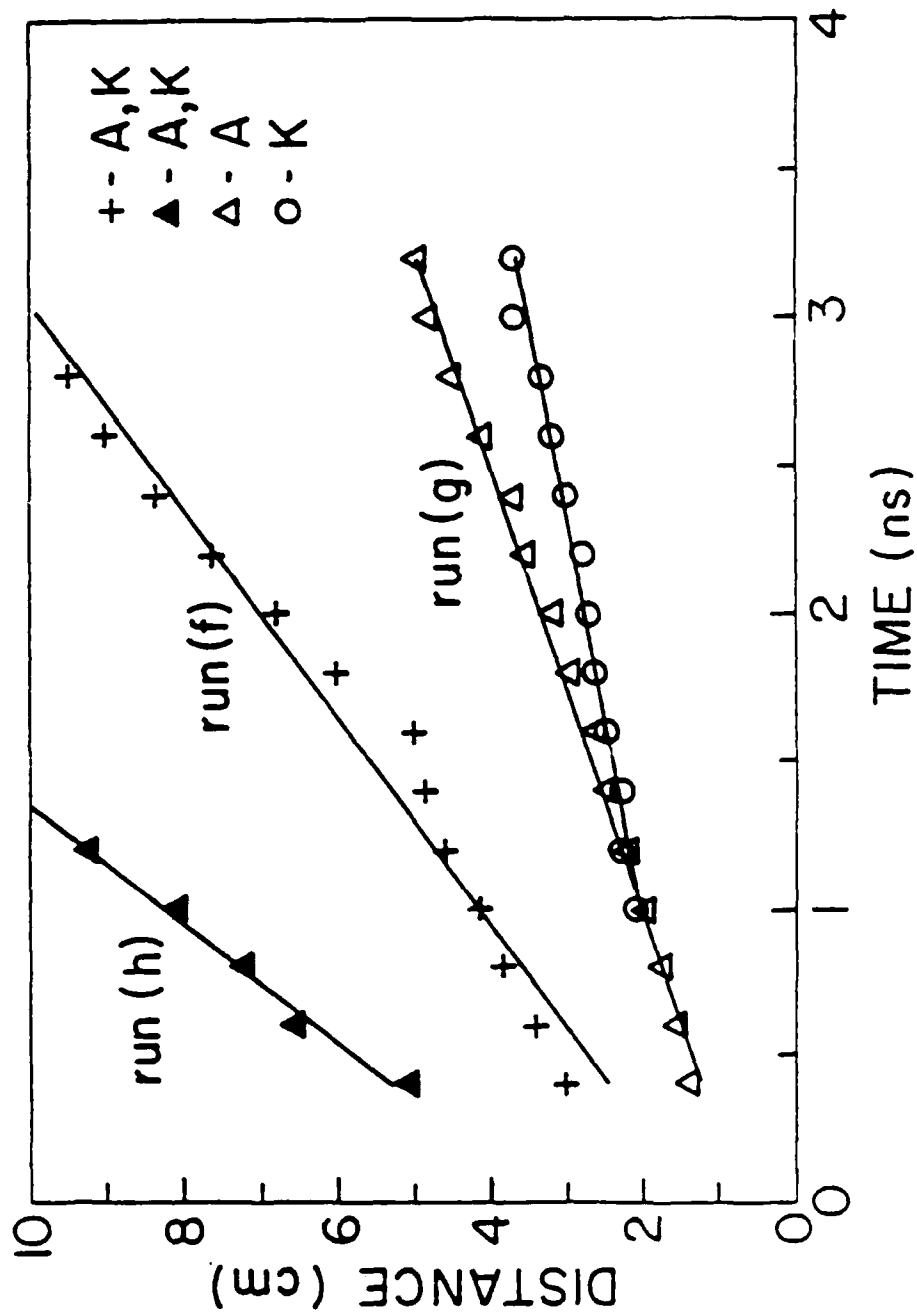


Fig. 4 Anode (A) and cathode (K) penetration as a function of time for runs (f)-(h) of Table I. The anode and cathode curves coincide in runs (f) and (h), but not at higher density, run (g).

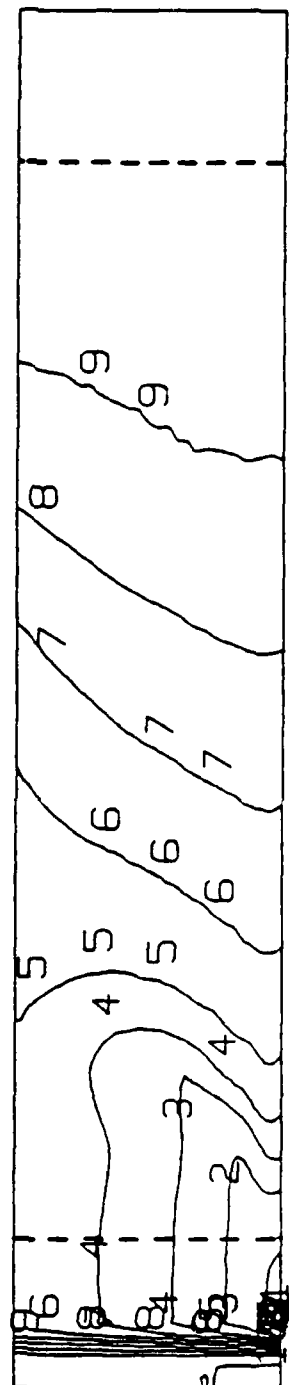
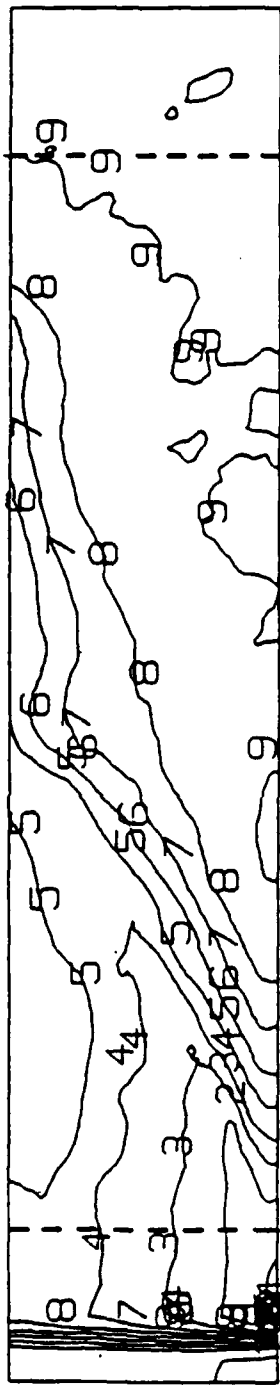


Fig. 5 Magnetic field contours for a collisionless (run (a) at top) and a collisional (run (f) at bottom) case at  $t = 2.4$  ns. Contour levels in both cases correspond and vary from  $-4.5$  kG (level 1) to  $-55.56$  G (level 9) with increment  $0.55$  kG per level.

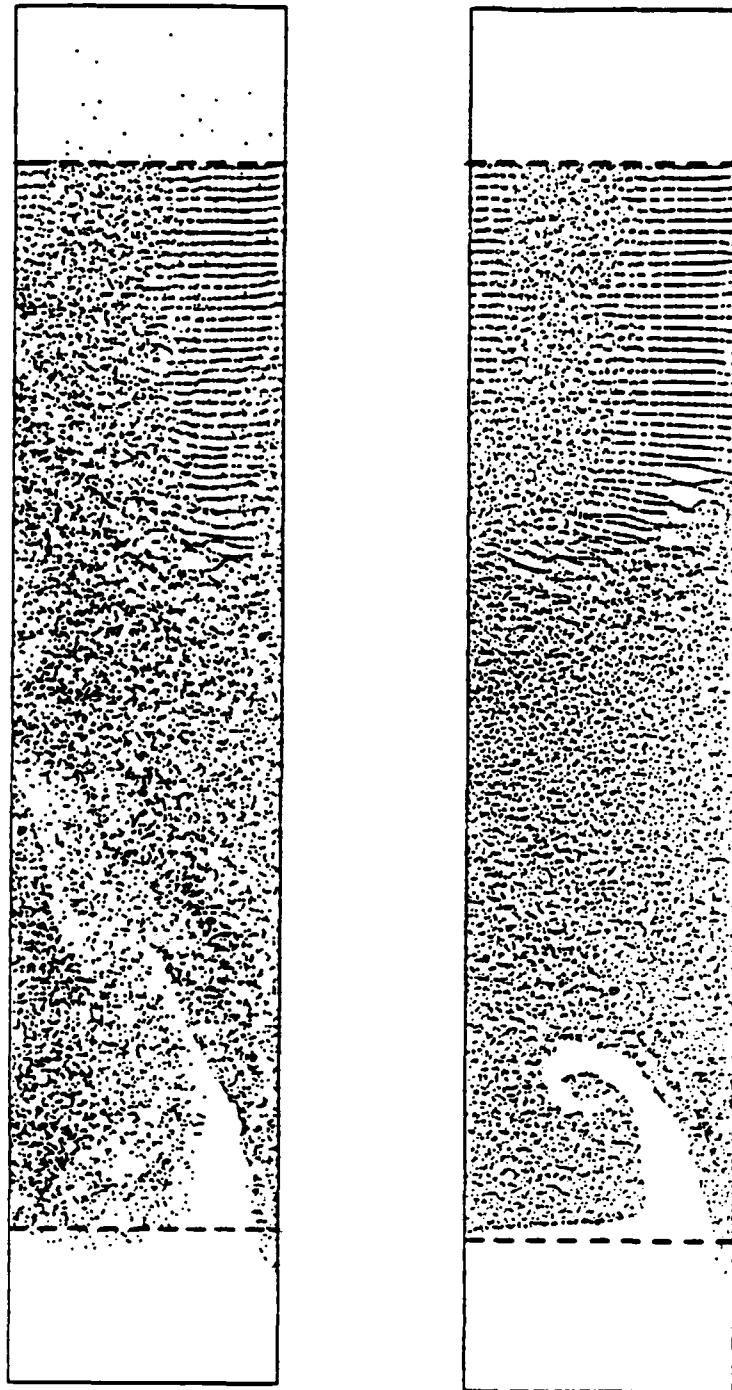


Fig. 6 Electron particle plots for a collisionless (run (a) at top) and a collisional (run(f) at bottom) case at  $t = 2.4$  ns.

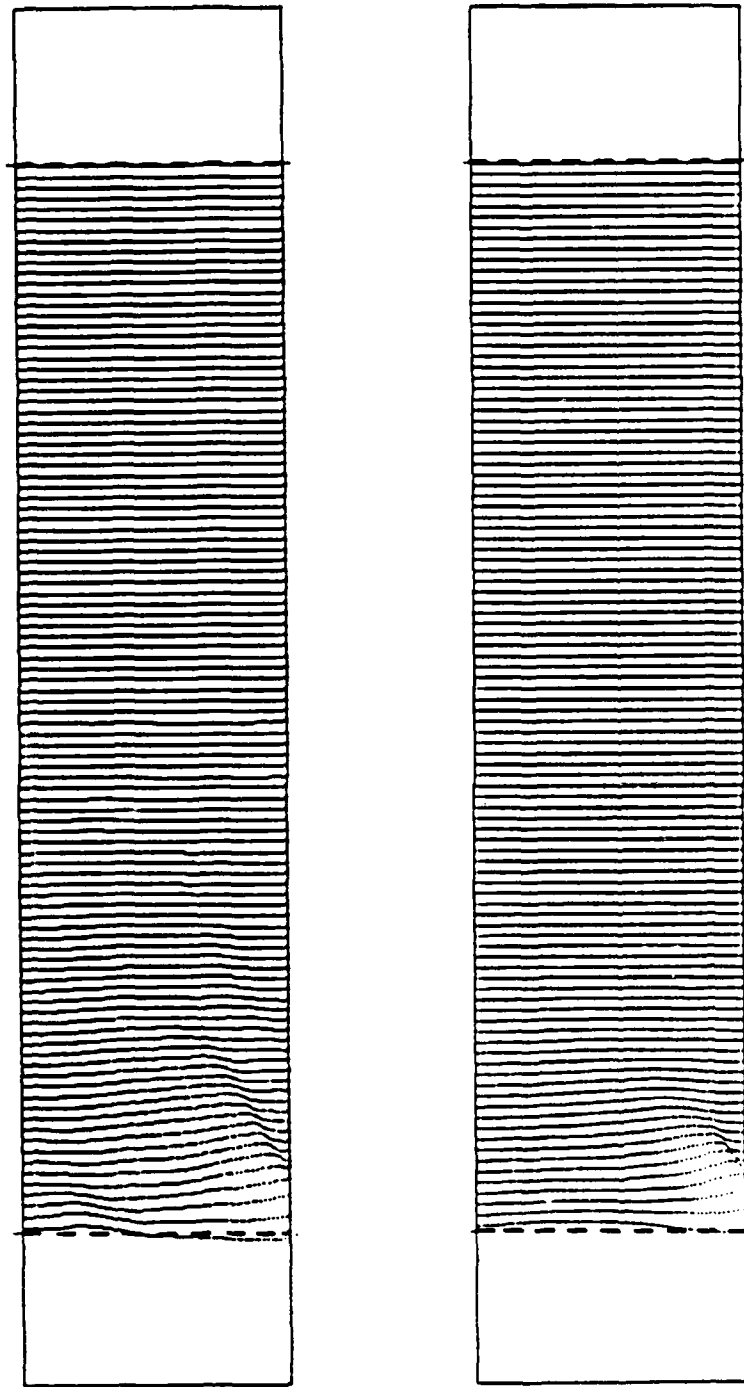


Fig. 7. Ion particle plots for a collisionless (run(a) at top) and a collisional (run (f) at bottom) case at  $t = 2.4$  ns.

DISTRIBUTION LIST FOR NRL MEMORANDUM REPORT NO. 6240

Los Alamos National Laboratory  
P.O. Box 1663  
Los Alamos, NM 87545  
Attn: Rodney Mason

Los Alamos National Laboratory  
P.O. Box 1663  
Los Alamos, NM 87545  
Attn: Michael Jones

Sandia National Laboratories  
P.O. Box 5800  
Albuquerque, NM 87185  
Attn: J. P. Quintenz/1241

Sandia National Laboratories  
P.O. Box 5800  
Albuquerque, NM 87185  
Attn: M.A. Sweeney/1265

Sandia National Laboratories  
P.O. Box 5800  
Albuquerque, NM 87185  
Attn: R. Stinnett/1264

Cornell University  
309 Upson Hall  
Ithaca, NY 14853  
Attn: R. Sudan

JAYCOR, Inc  
1011 Torreyana Road  
San Diego, CA 92121  
Attn: N. Krall

Princeton Plasma Physics Laboratory  
James Forrestal Campus  
P.O. Box 451  
Princeton, NJ 08540  
Attn: R. Kulsrud

Science Applications, Inc.  
1710 Goodridge Drive  
P.O. Box 1303  
McLean, VA 22101  
Attn: A. Drobot

Systems, Science and Software, Inc.  
P.O. Box 1620  
LaJolla, CA 92038  
Attn: A. R. Wilson

University of New Mexico  
Department of Chemical  
& Nuclear Engineering  
Albuquerque, NM 87131  
Attn: S. Humphries

University of New Mexico  
Department of Chemical  
& Nuclear Engineering  
Albuquerque, NM 87131  
Attn: N.F. Roderick

CEA, Centre de Etudes de Valduc  
P. B. 14  
21120 Is-sur-Tille  
France  
Attn: C. Bruno

Cullham Laboratories  
UKAEA  
Ebingdon, Birks.  
England  
Attn: N.J. Peacock

Ecole Polytechnique Labo. PM1  
91128 Palaseau Cedex  
France  
Attn: H. Doucet

Institut fur Neutronenphysik  
un Reaktortechnik  
Postfach 3640  
Kernforschungszentrum  
D-7500 Karlsruhe 1,  
Federal Republic of Germany  
Attn: H. Bluhm

Institut fur Neutronenphysik  
un Reaktortechnik  
Postfach 3640  
Kernforschungszentrum  
D-7500 Karlsruhe 1,  
Federal Republic of Germany  
Attn: H.U. Karow

Institut fur Neutronenphysik  
un Reaktortechnik  
Postfach 3640  
Kernforschungszentrum  
D-7500 Karlsruhe 1,  
Federal Republic of Germany  
Attn: W. Schmidt

Max-Planck-Institut fur Plasmaphysik  
8046 Garching bei Munchen  
Federal Republic of Germany  
Attn: I. Hofmann

University of New South Wales  
Dept. of Theoretical Physics  
P.O. Box 1  
Kensington, NSW 2033  
Australia  
Attn: H. Hora

U.S. Department of Energy  
Office of Inertial Fusion  
Washington, DC 20545  
Attn: S.L. Kahalas 1 copy  
R.L. Schriever 1 copy

U.S. Department of Energy  
Office of Classification  
Washington, DC 20545  
Attn: Robert T. Duff 1 copy

U.S. Department of Energy  
Nevada Operations Office  
P.O. Box 14100  
Las Vegas, NV 89114 2 copies

U.S. Department of Energy  
P.O. Box 62  
Oak Ridge, TN 37830 1 copy

Cornell University  
Ithaca, NY 14850  
Attn: D.A. Hammer 1 copy  
R.N. Sudan 1 copy

Defense  
Technical Information Center Station  
Duke Street  
Alexandria, VA 22314  
Attn: T.C. 2 copies

JAYCOR, Inc.  
1608 Spring Hill Rd.  
Vienna, VA 22180-2270  
Attn: B.V. Weber 1 copy  
D.D. Hinshelwood 1 copy

KMS Fusion, Inc.  
3941 Research Park Drive  
P.O. Box 1567  
Ann Arbor, MI 48106  
Attn: A.A. Glass 1 copy

Lawrence Berkley Laboratory  
Berkley, CA 94720  
Attn: D. Keefe 1 copy

Lawrence Livermore National Laboratory  
P.O. Box 808  
Livermore, CA 94550  
Attn: R. Batzel/J. Kahn, L-1 1 copy  
J. Emmett, L-488 1 copy  
W. Krupke, L-488 1 copy  
E. Storm, L-481 1 copy  
J. Lindl, L-477 1 copy

Los Alamos Scientific Laboratory  
P.O. Box 1663  
Los Alamos, NM 87545  
Attn: S.D. Rockwood,  
ICF Prog. Mgr.  
DAD/IF/M/S 527 1 copy

Naval Research Laboratory  
4555 Overlook Ave., S.W.  
Washington, D.C. 20375-5000  
Attn: Code/Name

2628/TID Dist	22 copies
1000/T. Coffey	1 copy
4000/W. Ellis	1 copy
4040/J. Boris	1 copy
4700/S.L. Ossakow	26 copies
4701/I. Vitkovitsky	1 copy
4710/C. Kapetanakos	1 copy
4720/J. Davis	1 copy
4730/S. Bodner	1 copy
4740/W. Manheimer	1 copy
4750/R. Meger	1 copy
4760/B. Robson	1 copy
4770/G. Cooperstein	10 copies
4770.1/F. Young	1 copy
4770.1/D. Mosher	1 copy
4770.2/R. Commisso	1 copy
4771/P. Ottinger	1 copy
4771/J. Neri	1 copy
4771/J. Grossmann	1 copy
4773/S. Stephanakis	1 copy
4790/D. Colombant	1 copy
4790/I. Haber	1 copy
4790/M. Lampe	1 copy
4600/D. Nagel	1 copy

Sandia National Laboratories  
P.O. Box 5800  
Albuquerque, NM 87185

Attn: J.P. VanDevender/1200 1 copy  
D.L Cook/1250 5 copies  
T. Martin/1250 1 copy

University of Rochester  
250 East River Road  
Rochester, NY 14623

Attn: J. Eastman 1 copy